ISSN NO. 2320-5407

Journal homepage: http://www.journalijar.com

INTERNATIONAL JOURNAL OF ADVANCED RESEARCH

RESEARCH ARTICLE

Formability of High Temperature and High Strain Rate Superplastic Deep Drawing Process for AA2219 Cylindrical Cups

A. Chennakesava Reddy

Professor, Department of Mechanical Engineering, JNTUH College of Engineering, Kukatpally, Hyderabad, India.

Manuscript Info

Manuscript History:

Received: 15 August 2015
Final Accepted: 22 September 2015
Published Online: October 2015

Key words:

AA2219, high temperature, high strain rate, superplastic deep drawing process, coefficient of friction, cylindrical cups, forming limit diagram.

Corresponding Author

A. Chennakesava Reddy

Abstract

High strain rate superplastic forming process is gaining importance in automotive and aerospace industry as it reduces manufacturing time. In this present work, a statistical approach based on Taguchi Techniques and finite element analysis were adopted to determine the formability of cylindrical cup using high strain rate deep drawing process. The process parameters were temperature, strain rate, coefficient of friction and blank holder velocity. The FEA results obtained using finite element software namely D-FORM were validated through the experimental results. The AA2219 sheets were used for the deep drawing of the cylindrical cups. The strain hardening exponent was 0.36 at strain rate of 5.0 s^{-1} and temperature of 400^{o}c. The formability of the cups was outstanding for the surface expansion ratio in the range of 1.6 to 2.5. The temperature and strain rate have substantial effects on the effective stress and the height of the cups drawn.

INTRODUCTION

The aerospace and automotive industry is increasingly employing superplastic forming of aluminum alloys. Fine grain size is a key requirement for materials to exhibit superplastic behavior. At higher temperatures, superplastic alloys can be deformed by several times of their initial size without fracture. The conventional superplastic forming is carried out at low strain rates, typically about $10^{-4} – 10^{-3}$ s^{-1} and high forming temperatures. Superplastic forming (SPF) process depends on the phenomena of grain boundary sliding, dislocation creep and grain boundary diffusion as stated by Clarisse et al. (1999). Among aluminum alloys, currently, AA1050, AA1100, AA2004, AA5083 and AA7475 are being used for super forming components. Numerous investigations (Hecht and Kannan., 1995; Patnakar and Jen., (1998); Reddy; 2015) have been carried out to enhance the superplastic properties of aluminum alloys. The significance of high strain rate superplastic (HSRS) forming process is to reduce the forming time. The superplastic regime is dislocated to faster strain rates when the grain size of a material is reduced.

Deep drawing is a large deformation elasto-plastic problem. In large deformation elasto-plastic problems, the response of the body becomes non-linear. One of the commonly used formulations for such problems is the updated Lagrangian formulation where the analysis is carried out in an incremental manner. Common deep drawn products are cans, boxes, and bottles, as well as irregularly shaped products. Parts fabricated by hot deep drawing process are characterized by high strength and complex shapes. The drawbacks of conventional deep drawing are blockage for some industrial applications. In conventional deep drawing process, radial drawing stress and tangential compressive stress can cause wrinkling or fracturing. In metal forming processes, the friction influences the strain distribution at tool blank interface and drawability of metal sheet. In an experimental work carried out on the warm deep drawing process of the EDD steel, the thinning at punch corner radius is found to be lesser at 2000C (Reddy et al., 2012). In another work performed by the author (2012) on the cup drawing process using an implicit finite element analysis, the thinning is observed high strains at the thinner sections of cup walls. In the finite element

simulations, a forming limit diagram (FLD) has been successfully applied to analyze the fracture phenomena by comparing the strain status (Shehata et al., 1978).

Even though extensive studies have been conducted on superplastic as well as high strain rate superplastic forming processes on aluminum alloys, high temperature and high strain rate superplastic forming has not found in the literature. The significance of the present work was to find fitness of AA2219 aluminum alloy for high temperature and high strain rate superplastic forming process. In the present work, the formability of high temperature and high strain rate (HTHSR) superplastic deep drawing process was assessed during the fabrication of AA2219 cylindrical cups. The investigation was focused on the process parameters such as temperature, strain rate, coefficient of friction and blank holder velocity. The design of experiments was carried out using Taguchi technique and HTHSR superplastic deep drawing process was executed using the finite element analysis software namely D-FORM 3D. The results obtained through the finite element analysis were validated experimentally.

1. MATERIALS AND METHODS

AA2219 aluminum alloy consists of: Cu (6%), Zr (0.2%), V (0.15%), Ti (0.5%), Si (≤ 0.2%), Mg (≤ 0.02%), Mn (≤ 0.3%), Fe (≤ 0.3%), Zn (≤ 0.1%) and Al (92 – 93%). In the present work, AA2219 was used to fabricate cylindrical cups. The levels chosen for the controllable process parameters are summarized in table 1. Each of the process parameters was studied at three levels. The orthogonal array (OA), L9 was selected to carry out experimental and finite element analysis (FEA). The assignment of parameters in the OA matrix is given in table 2.

2.1 Fabrication and Testing of Deep Drawn Cups

The sheets of AA2129 were cut to the required blank size as defined by Reddy (2015). The blank specimens were heated in a muffle furnace to the desired temperature as per the design of experiments. The blank force was calculated using Eq. (1). The cups were fabricated using hydraulically operated deep drawing machine. The Erichsen deep drawing test was conducted for testing the deep drawing quality and ear forming tendency on AA2219 aluminum alloy sheet. The test consisted of forming an indentation by pressing a punch with a spherical end against a test piece clamped between a blank holder and a die, until a through crack appears. The depth of the cup was measured.

Drawing force, $F_d = \pi dt[D/d - 0.6]\sigma_y$ (1)

Clearance, $c = t \pm \mu\sqrt{10t}$ (2)

2.2 Finite Element Analysis

The finite element modeling and analysis was carried using D-FORM 3D software. The cylindrical sheet blank was created with desired diameter and thickness using CAD tools. The cylindrical top punch, cylindrical bottom hollow die were also modeled with appropriate inner and outer radius and corner radius using CAD tools. The clearance between the punch and die was calculated as in Eq. (2). The sheet blank was meshed with tetrahedral elements. The modeling parameters of deep drawing process were as follows:

Number of tetrahedron elements for the blank: 9810
Number of polygons for top die: 9120
Number of polygons for bottom die: 9600
Number of polygons for moving blank die: 960

In the present work, moving blank die was used to hold the blank at a predefined speed different to the punch speed. The contact between blank/punch and die/blank were coupled as contact pair (figure 1). The mechanical interaction between the contact surfaces was assumed to be frictional contact and modeled as Coulomb's friction model. The finite element analysis was chosen to find the metal flow, effective stress, height of the cup, and damage of the cup. The finite element analysis was carried out using D-FORM 3D software according to the design of experiments.

2. RESULTS AND DISCUSSION

Each experiment was repeated twice. For the ANOVA (analysis of variance) the Fisher's test (F = 3.01) was carried out on all the parameters (A, B, C and D) at 90% confidence level.

3.1 Influence of process parameters on effective stress

The percent contributions of A, B, C and D vary in a large range between 4.55% and 60.49% towards the total variation in the effective stress (Table 3). The temperature (A) by itself has a major effect (60.49%) on the effective stress. The coefficient of friction (B) can cause 20.90% of total variation in the effective stress. The strain rate (C) and blank holder (BH) velocity (D) have contributed, respectively, 4.55% and 12.20% of the total variation in the effective stress.

Figure 2a presents the effective stress induced in AA2129 alloy during cup drawing process as a function of temperature. The effective stress was 164.0 MPa and 195.5 MPa at the lowest (300^{o}C) and highest (500^{o}C) operating temperatures; it was 154.5 MPa at temperature of 400^{o}C. The recrystallization temperature of AA2129 is about 400^{o}C. When the temperature went beyond recrystallization temperature, the grains might be elongated in the direction parallel to the direction of applied force (tensile). The material got strain hardened, i.e. its yield strength, tensile strength and von Mises stress were increased. This might be the reason for the increase of von Mises stress above 400^{o}C.

Figure 2b depicts the effective stress as a coefficient of friction. As the coefficient of friction varied from 0.1 to 0.15, the effective stress increased from 156.83 MPa to 180.17 MPa and its value was unchanged notably above 0.2 value of coefficient of friction. In deep drawing process, friction initiates from sliding contact between the tool and the blank sheet. In the initial stages of high strain rate deformation, the friction dominates to limit the stretch deformation. Consequently, the effective stress increases due to the requirement of high force for the material to undergo plastic deformation. The surface asperities of the blank sheet undergo stretch deformation on account of the tangential load along the sliding contact. Once the surface asperities become flattened due to stretch deformation (figure 3), further increase of friction does not demand the hike of drawing force and subsequent rise in the effective stress during high strain rate deforming process. This might be the phenomenon occurred at extreme values of coefficient of friction during high strain rate deforming process.

In general, the flow stress increases with the increase of strain rate. In every instance, the effective stress was increased with increasing strain rate during the initial stages of deformation as observed from figure 2c. On the other hand, having reached a peak value, the stress was reduced on further increase of strain rate. This reduction in stress took place when the strain and strain rate hardening effects were outweighed by the softening effect as result of the heat generated during plastic deformation. A general expression for flow stress, encompassing temperature, strain, strain rate, recrystallization has been given in the form:

$$\sigma = \frac{2}{\sqrt{3(1-m)}} K \varepsilon^{n} \dot{\varepsilon}^{m} exp(1-\beta T) \quad (3)$$

n is strain hardening exponent, m is strain rate sensitivity exponent, T is temperature.

Figure 2d depicts the effective stress as a function of blank holder velocity. In the present work, the blank holder was allowed to move along with the punch but at different velocities. As the blank holding force was maintained constant in this work, the blank holder would come in contact with the blank early due to increased blank holder velocity and consequently, the material was restrained to the plastic deformation and the metal flow into the die. As a result, the effective stress increased with the increase of blank holder velocity from 0.4 to 0.8 mm/s.

The FEA results of effective stress are shown in figure 4 for various test conditions as per the design of experiments. For trials 1, 2 and 3, the temperature was 300^{o}C and other process parameters were varied as mentioned in tables 1 and 2. The effective stresses for trails 1, 2 and 3 were, respectively, 137 MPa, 186 MPa and 176 MPa (figure 4a). For trials 7, 8 and 9, the temperature was 500^{o}C and other process parameters were as designed in tables 1 and 2. The effective stresses for trails 7, 8 and 9 were, respectively, 192 MPa, 197 MPa and 193 MPa (figure 4c). With regard to coefficient of friction and strain rate, this trend is matching with that shown in figures 2b and 2c. For trials 4, 5 and 6, the temperature was 400^{o}C and other process parameters were as stated in tables 1 and 2. The effective stresses for trails 4, 5 and 6 were, respectively, 183 MPa, 155 MPa and 165 MPa (figure 4b). This trend was contradictory to that mentioned in figures 2b and 2c due to superseding effect of the temperature over the strain rate. This behavior might be attributed to the combined of three independent deformation mechanisms such as grain growth, grain boundary sliding and dislocation creep.

3.2 Influence of Process Parameters on Surface Expansion Ratio

In the deep drawing process the plastic deformation in the surface is much more pronounced than in the thickness. The author (2015) introduces the term surface expansion ratio to measure the formability of cups. The ANOVA summary of surface expansion ratio is given in table 4. As per the Fisher's test (F = 3.01), the temperature, (A),

coefficient of friction (B), strain rate (C) and BH velocity (D) could contribute, respectively, 27.25%, 23.65%, 15.35% and 30.34% respectively towards the total variation in the surface expansion ratio.

The surface expansion ratio would increase with an increase in the operating temperature from 300^{o}C to 400^{o}C and later on it would decrease for the increase of temperature from 400^{o}C to 500^{o}C (figure 5a). The lowest operating temperature of 300^{o}C might be too low for dynamic recrystallization to take place and then low surface expansion was resulted. The low surface expansion at the highest operating temperature of 500^{o}C was beyond doubt due to excessive grain growth since the grain size at the punch radius section of the sample was measured as/40 µm. The surface expansion ratio was high for the coefficient of friction of 0.15 due to stretch deformation (figure 5b). The effect of strain rate on the surface expansion ratio is shown in figure 5c. The surface expansion ratio increased with increase in the strain rate. High strain rate sensitivity is typically associated with a fine grain microstructure. The strain rate sensitivity of metals arises from the viscous nature of the deformation process. The surface expansion ratio was decreased with the blank holder velocity (figure 5d). At high velocities, the blank holder would come in contact with the blank early and accordingly, the material was restrained to flow into the die resulting reduction in the surface expansion.

The FEA results of surface expansion ratio are revealed in figure 6 for various test conditions as per the design of experiments. For the surface expansion ratio in the range of 1.6 – 2.50 (figure 6), the height of the cups was between 72.0 to 75.0 mm (figure 7). For the remaining trails the surface expansion ratios were higher than 2.5 yielding the cup height in the range of 37 to 67 mm.

3.3 Forming Limit Diagrams and Damages in the Cups

Figure 8 depicts the forming limit diagram (FLD) with damages in the cylindrical cups drawn from AA2219 sheets at temperature 300^{o}C. The first branch covers the range from equal bi-axial tension to plane strain. The second branch corresponds to plane strain and uniaxial tension. The third branch extends from uniaxial tension to pure shear. The fourth branch widens from pure shear to uniaxial compression. The FLD for the cylindrical cup drawn under trial 1 is located in the third and fourth branches. The cup drawn with trial 1 had wrinkles as the minor strain was twice the major strain induced in the blank material. The fracture has occurred in the cups drawn with trials 2 and 3 due to shear and uniaxial tension. For cups drawn with trials 2 and 3, the major strain was greater than the minor strain. Figure 9 illustrates the forming limit diagram and damages in the cups drawn from AA2219-H18 sheets with trials, 4, 5 and 6 at temperature 400^{o}C. Cups drawn on trial 4 were experienced with high uniaxial tension and stretching. Cups drawn from trials 5 and 6 were fractured due to shear, uniaxial tension and stretching. Cups drawn from trial 7 were experienced with uniaxial tension and biaxial tension. The cups were torn in the flange area owing to equal biaxial tension. Cups drawn under trial 8 were fractured in the flange region due to shear and stretching (figure 10). Cups drawn under trial 9 were fractured due to shear, uniaxial and stretching.

The damage factor was 33.50 and 20.90, respectively, observed with trial 5 and 9 conditions (figure 11). The experimental results confirm this situation. Coarse grains were observed in the cups drawn from trials 5 and 9 (figure 12). The Erichsen cup results also validate these phenomena. The damage factor was least with trail conditions 1, 7 and 8. Fine grains were revealed in the cups drawn from trials 7.

3. CONCLUSIONS

With strain rate of 5.0 s^{-1}, the surface expansion ratio of the cup drawn was high. The effective stress was least at operating temperature of 400^{o}C. The reason for the failure of cups was due to uniaxial tension and shear. The strain hardening exponent (n) was 0.36 for the strain rate of 5.0 s^{-1} and operating temperature of 400^{o}C. AA2219 has been found to yield successful cup at low temperature and high strain rate as well as high temperature and high strain rate.

ACKNOWLEDGMENT

The author wishes to thank University Grants Commission (UGC), New Delhi, India for financial assisting this project.

Table 1: Control parameters and levels

Factor	Symbol	Level–1	Level–2	Level–3
Temperature, ^{0}C	A	300	400	500
Coefficient of friction	C	0.10	0.15	0.20
Strain rate, 1/s	B	1	3	5
BH velocity, mm/s	D	0.4	0.6	0.8

Table 2: Orthogonal array (L9) and control parameters

Treat No.	A	B	C	D
1	1	1	1	1
2	1	2	2	2
3	1	3	3	3
4	2	1	2	3
5	2	2	3	1
6	2	3	1	2
7	3	1	3	2
8	3	2	1	3
9	3	3	2	1

Table 3: ANOVA summary of the effective stress

Source	Sum 1	Sum 2	Sum 3	*SS*	*v*	*V*	*F*	*P*
A	984.00	927.00	1173.00	5527.00	2	2763.50	30.71	60.49
B	941.00	1081.00	1062.00	1922.34	2	961.17	10.68	20.90
C	987.00	1055.00	1042.00	434.34	2	217.17	2.41	4.55
D	967.00	1083.00	1034.00	1130.34	2	565.17	6.28	12.20
e				89.98	9	10.00	0.11	1.86
T	3879.00	4146.00	4311.00	9104.00	17			100.00

Note: *SS* is the sum of square, *v* is the degrees of freedom, *V* is the variance, *F* is the Fisher's ratio, *P* is the percentage of contribution and *T* is the sum squares due to total variation.

Table 4: ANOVA summary of the surface expansion ratio

Source	Sum 1	Sum 2	Sum 3	*SS*	*v*	*V*	*F*	*P*
A	13.79	24.86	14.18	13.14	2	6.57	7.65	27.25
B	11.87	23.58	17.38	11.43	2	5.72	6.66	23.65
C	13.24	16.94	22.65	7.49	2	3.75	4.36	15.35
D	25.24	13.88	13.71	14.56	2	7.28	8.47	30.24
e				0.8593	9	0.1	0.12	3.51
T	64.14	79.26	67.92	47.4793	17			100

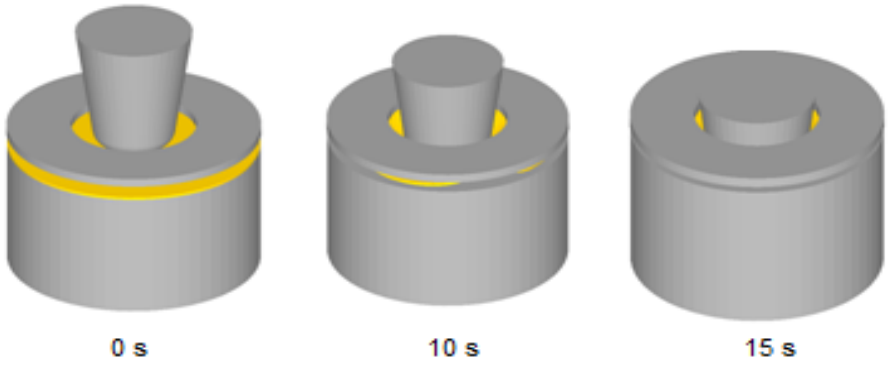

Figure 1: Cylindrical cup drawing at different steps.

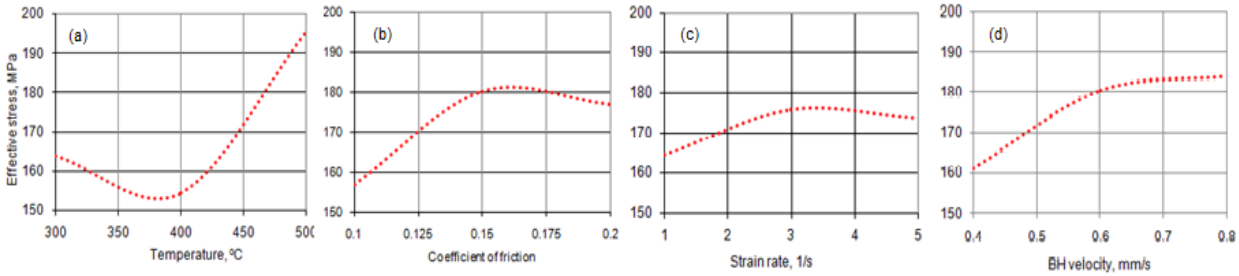

Figure 2: Influence of process parameters: (a) temperature, (b) coefficient of friction (c) strain rate and (d) BH velocity on effective stress.

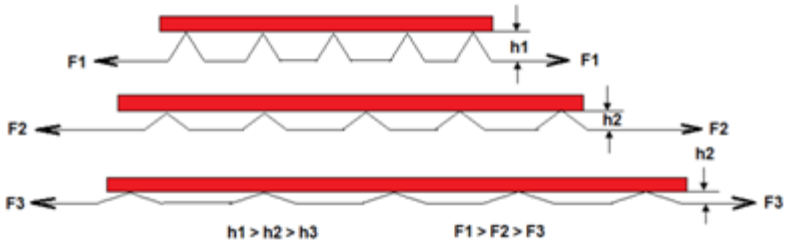

Figure 3: Illustration of stretch deformation

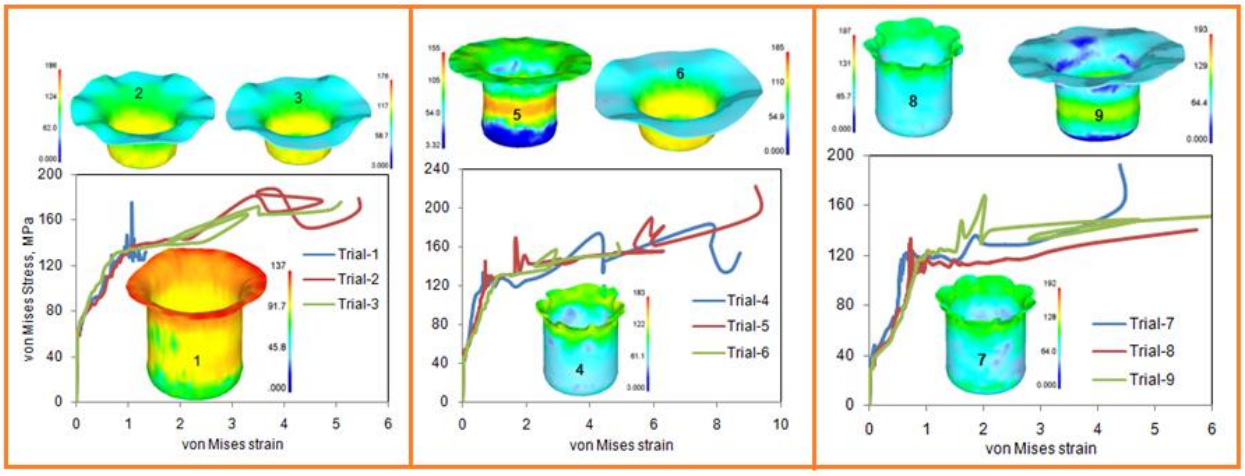

Figure 4: Effect of process parameters on the effective stress.

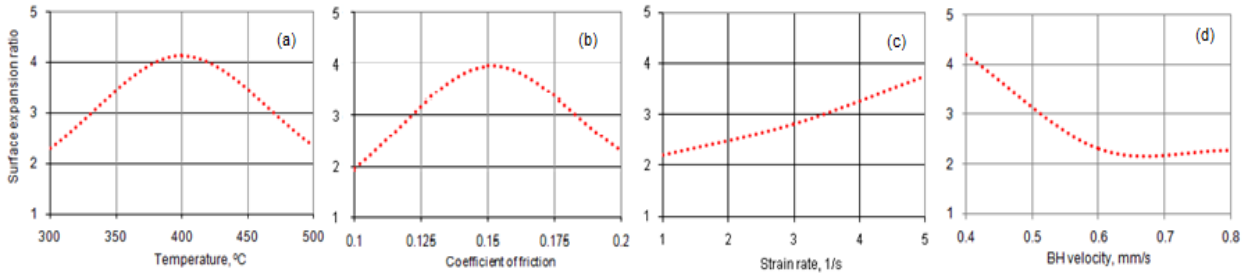

Figure 5: Influence of process parameters: (a) temperature, (b) coefficient of friction (c) strain rate and (d) BH velocity on surface expansion ratio.

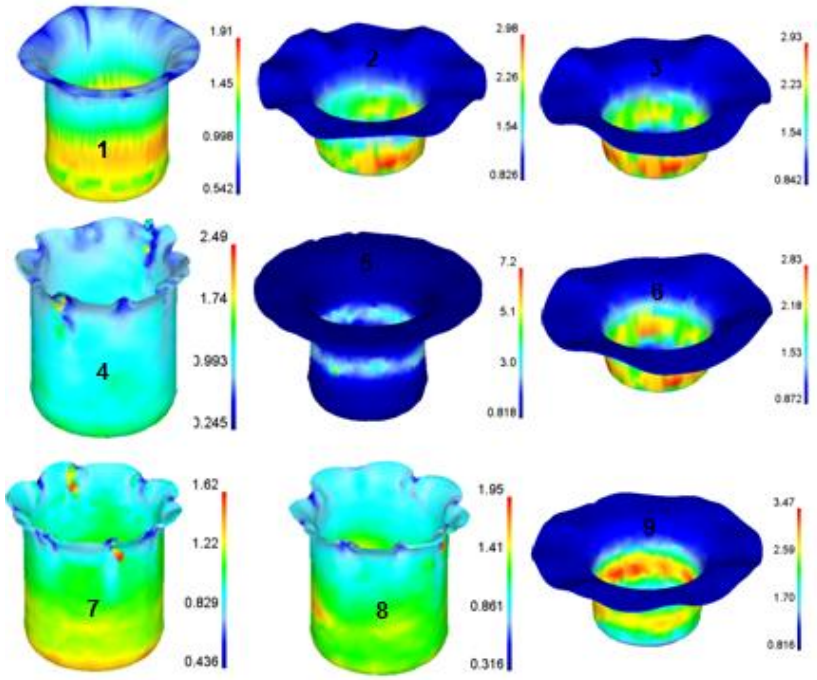

Figure 6: Effect of process parameters on the surface expansion ratio.

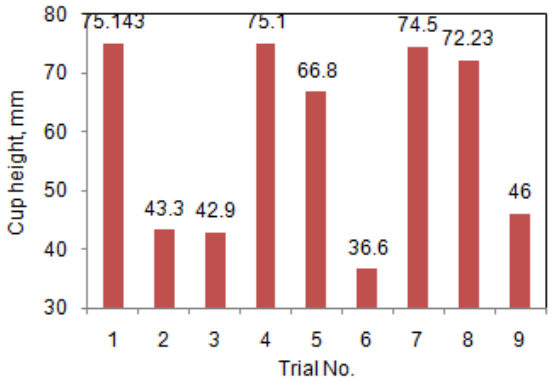

Figure 7: Cup heights under different trials.

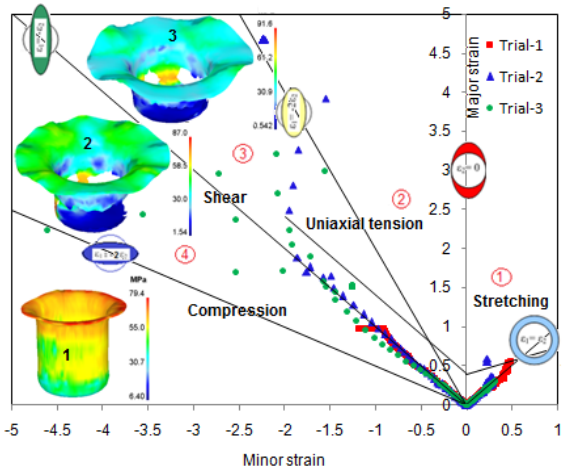

Figure 8: Forming limit diagram with damage in the cups drawn at temperature 300°C.

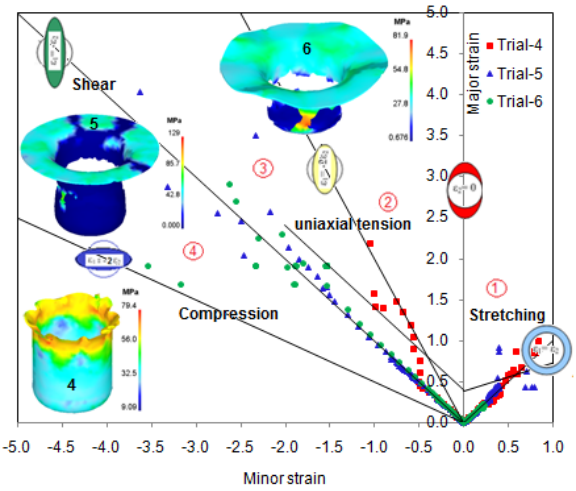

Figure 9: Forming limit diagram with damage in the cups drawn at temperature 400°C.

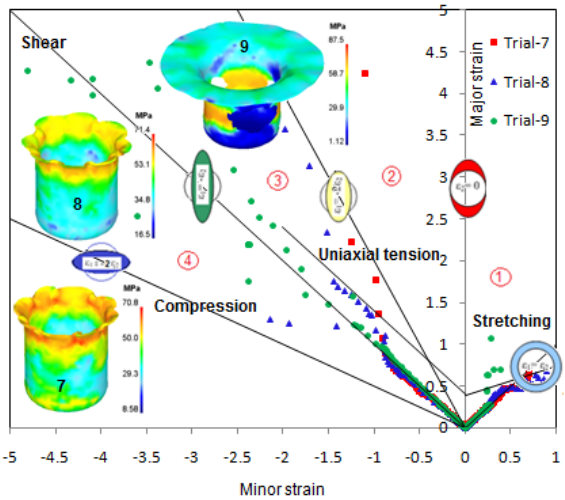

Figure 10: Forming limit diagram with damage in the cups drawn at temperature 500°C.

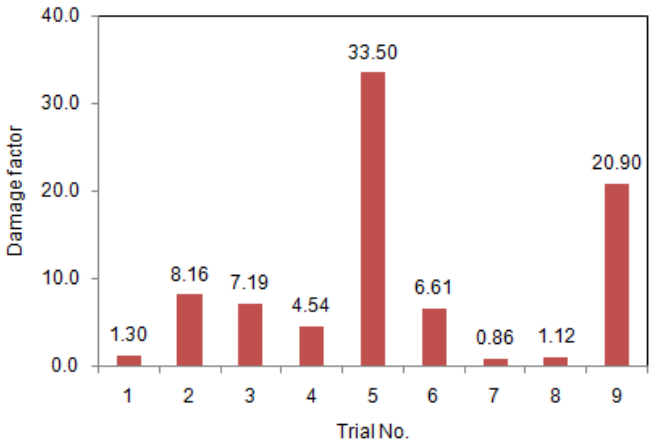

Figure 11: Damage factors under different trials.

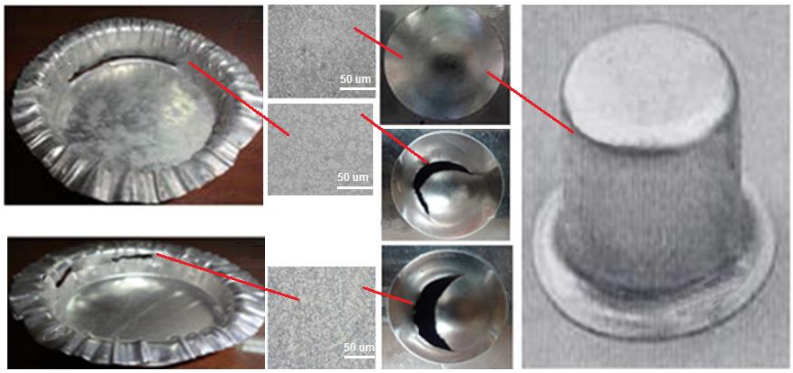

Figure 12: Experimental validation of FEA results

References

Chennakesava Reddy, A., Kishen Kumar Reddy, T., Vidya Sagar, M. (2012). Experimental characterization of warm deep drawing process for EDD steel, Int. J. of Multidisciplinary Res. & Adv. Eng. 4:53-62.

Chennakesava Reddy, A. (2012). Evaluation of local thinning during cup drawing of gas cylinder steel using isotropic criteria, Int. J. of Eng. & Mat. Sci., 5:71-76.

Chennakesava Reddy, A. (2015). Formability of superplastic deep drawing process with moving blank holder for AA1050-H18 conical cups, Int. J. of Res. in Eng. and Technol., 4(8):124-132.

Chennakesava Reddy, A. (2015). Finite Element Analysis of Warm Deep Drawing Process for 2017T4 Aluminum Alloy: Parametric Significance Using Taguchi Technique, Int. J. of Advanced Res., 3(5):1247-1255.

Clarisse, L., Bataille, A., Pennec, Y., Crampon, J., Duclos, R. (1999). Investigation of grain boundary sliding during superplastic deformation of a fine-grained alumina by atomic force microscopy, Ceramics Int., 25:389-394.

Hecht, R.L., Kannan, K. (1995). in: A.K. Gosh, T.R. Bieler (Eds.), Superplasticity and Superplastic Forming, TMS, Warrendale, PA, USA, 1995, p. 259.

S.N. Patankar, T.M. Jen.(1998). Strain Rate Insensitive Plasticity in Aluminum Alloy 5083, Scripta Mater. 38:1255-1261.

Shehata, F., Painter, M. J., Pearce, R. (1978). Warm forming of aluminum/magnesium alloy sheet, J.of Mecha. Working Technol., 2:279-291.